

# A dusty star-forming galaxy at $z = 6$ revealed by strong gravitational lensing

Jorge A. Zavala<sup>1,2\*</sup>, Alfredo Montaña<sup>3</sup>, David H. Hughes<sup>1</sup>, Min S. Yun<sup>4</sup>, R. J. Ivison<sup>5,6</sup>, Elisabetta Valiante<sup>7</sup>, David Wilner<sup>8</sup>, Justin Spilker<sup>9</sup>, Itziar Aretxaga<sup>1</sup>, Stephen Eales<sup>7</sup>, Vladimir Avila-Reese<sup>10</sup>, Miguel Chávez<sup>1</sup>, Asantha Cooray<sup>11</sup>, Helmut Dannerbauer<sup>12,13</sup>, James S. Dunlop<sup>6</sup>, Loretta Dunne<sup>6,7</sup>, Arturo I. Gómez-Ruiz<sup>3</sup>, Michał J. Michałowski<sup>14</sup>, Gopal Narayanan<sup>4</sup>, Hooshang Nayyeri<sup>11</sup>, Ivan Oteo<sup>6,5</sup>, Daniel Rosa González<sup>1</sup>, David Sánchez-Argüelles<sup>1</sup>, F. Peter Schloerb<sup>4</sup>, Stephen Serjeant<sup>15</sup>, Matthew W. L. Smith<sup>7</sup>, Elena Terlevich<sup>1</sup>, Olga Vega<sup>1</sup>, Alan Villalba<sup>1</sup>, Paul van der Werf<sup>16</sup>, Grant W. Wilson<sup>4</sup> and Milagros Zeballos<sup>1</sup>

**Since their discovery, submillimetre-selected galaxies<sup>1,2</sup> have revolutionized the field of galaxy formation and evolution. From the hundreds of square degrees mapped at submillimetre wavelengths<sup>3-5</sup>, only a handful of sources have been confirmed to lie at  $z > 5$  (refs<sup>6-10</sup>) and only two at  $z \geq 6$  (refs<sup>11,12</sup>). All of these submillimetre galaxies are rare examples of extreme starburst galaxies with star formation rates of  $\gtrsim 1,000 M_{\odot} \text{ yr}^{-1}$  and therefore are not representative of the general population of dusty star-forming galaxies. Consequently, our understanding of the nature of these sources, at the earliest epochs, is still incomplete. Here, we report the spectroscopic identification of a gravitationally amplified ( $\mu = 9.3 \pm 1.0$ ) dusty star-forming galaxy at  $z = 6.027$ . After correcting for gravitational lensing, we derive an intrinsic less-extreme star formation rate of  $380 \pm 50 M_{\odot} \text{ yr}^{-1}$  for this source and find that its gas and dust properties are similar to those measured for local ultra luminous infrared galaxies, extending the local trends to a poorly explored territory in the early Universe. The star-formation efficiency of this galaxy is similar to those measured in its local analogues<sup>13</sup>, despite a  $\sim 12$  Gyr difference in cosmic time.**

HATLAS J090045.4+004125 ( $\alpha = 09 \text{ h } 00 \text{ m } 45.8 \text{ s}$ ,  $\delta = +00^{\circ} 41' 23''$ ; hereafter G09 83808, since it was detected in the Galaxy and Mass Assembly 09 hrs field) is part of a sub-sample of the Herschel ATLAS '500  $\mu\text{m}$ -riser' galaxies<sup>14</sup> with ultra-red far-infrared (FIR) colours of  $S_{500\mu\text{m}} / S_{250\mu\text{m}} > 2$  and  $S_{500\mu\text{m}} / S_{350\mu\text{m}} > 1$ , with a flux density threshold of  $S_{500\mu\text{m}} < 80 \text{ mJy}$ . The FIR colours of this source are consistent with thermal dust emission redshifted to  $z > 4$  and represent a relatively simple selection criterion to find high-redshift galaxies. A similar selection allowed the identification of

HFLS3 (ref. <sup>11</sup>), an extreme starburst galaxy (even after corrected for gravitational amplification<sup>15</sup>) at  $z = 6.3$ , in the Herschel Multi-tiered Extragalactic Survey<sup>3</sup>.

G09 83808 was observed, among other ultra-red Herschel dusty star-forming galaxies, as part of a follow-up programme with the Large Millimeter Telescope Alfonso Serrano (LMT) using the AzTEC camera to obtain higher angular resolution ( $\sim 8.5$  arcsec) continuum observations at 1.1 mm. A sub-sample of those galaxies detected as a single source in the AzTEC images (that is, with no evidence of multiple components) and with photometric redshifts of  $z > 4$ , was selected for spectroscopic observations in the 3 mm band using the Redshift Search Receiver (RSR) on the LMT. In the LMT/RSR spectrum of G09 83808, we identified three emission lines corresponding to  $^{12}\text{CO}(6-5)$ ,  $^{12}\text{CO}(5-4)$  and  $\text{H}_2\text{O}(2_{11}-2_{02})$  (see Fig. 1). Based on these lines, we unambiguously determined the galaxy redshift to be  $z = 6.0269 \pm 0.0006$  (that is, when the Universe was just 900 million years old). Follow-up observations with the Submillimeter Array (SMA) telescope confirmed this solution through the detection of the redshifted [CII] ionized carbon line at 270.35 GHz (see Fig. 1).

High-angular resolution observations ( $0.24 \times 0.13$  arcsec, corresponding to a physical scale of  $\sim 1$  kpc at this redshift) taken with the Atacama Large Millimeter/submillimeter Array (ALMA; see Methods) at  $\sim 890 \mu\text{m}$  revealed a double arc structure (in a partial Einstein ring configuration of radius  $\sim 1.4$  arcsec) around a foreground galaxy at  $z = 0.776$  (see Fig. 2), implying strong gravitational amplification of the high-redshift background galaxy. Using these ALMA continuum observations to constrain the effects of gravitational lensing, modelling directly the visibilities in the  $uv$  plane (see Methods for additional details), we derived a gravitational

<sup>1</sup>Instituto Nacional de Astrofísica, Óptica y Electrónica, Luis Enrique Erro 1, 72840 Puebla, Mexico. <sup>2</sup>Department of Astronomy, The University of Texas at Austin, 2515 Speedway Boulevard, Austin, TX 78712, USA. <sup>3</sup>Consejo Nacional de Ciencia y Tecnología-Instituto Nacional de Astrofísica, Óptica y Electrónica, Luis Enrique Erro 1, 72840 Puebla, Mexico. <sup>4</sup>Department of Astronomy, University of Massachusetts, Amherst, MA 01003, USA. <sup>5</sup>European Southern Observatory, Karl Schwarzschild Strasse 2, Garching bei München 85748, Germany. <sup>6</sup>Institute for Astronomy, University of Edinburgh, Royal Observatory, Blackford Hill, Edinburgh EH9 3HJ, UK. <sup>7</sup>School of Physics and Astronomy, Cardiff University, The Parade, Cardiff CF24 3AA, UK. <sup>8</sup>Harvard-Smithsonian Center for Astrophysics, 60 Garden Street, Cambridge, MA 02138, USA. <sup>9</sup>Steward Observatory, University of Arizona, 933 North Cherry Avenue, Tucson, AZ 85721, USA. <sup>10</sup>Instituto de Astronomía, Universidad Nacional Autónoma de México, Ciudad Universitaria, 04510 CDMX, Mexico. <sup>11</sup>Department of Physics and Astronomy, University of California, Irvine, CA 92697, USA. <sup>12</sup>Instituto de Astrofísica de Canarias, E-38205 La Laguna, Tenerife, Spain. <sup>13</sup>Universidad de La Laguna, Departamento de Astrofísica, E-38206 La Laguna, Tenerife, Spain. <sup>14</sup>Astronomical Observatory Institute, Faculty of Physics, Adam Mickiewicz University, Stoleczna 36, 60-286 Poznań, Poland. <sup>15</sup>Department of Physical Sciences, The Open University, Milton Keynes MK7 6AA, UK. <sup>16</sup>Leiden Observatory, Leiden University, PO Box 9513, NL-2300 RA Leiden, The Netherlands. \*e-mail: [zavala@inaoep.mx](mailto:zavala@inaoep.mx)

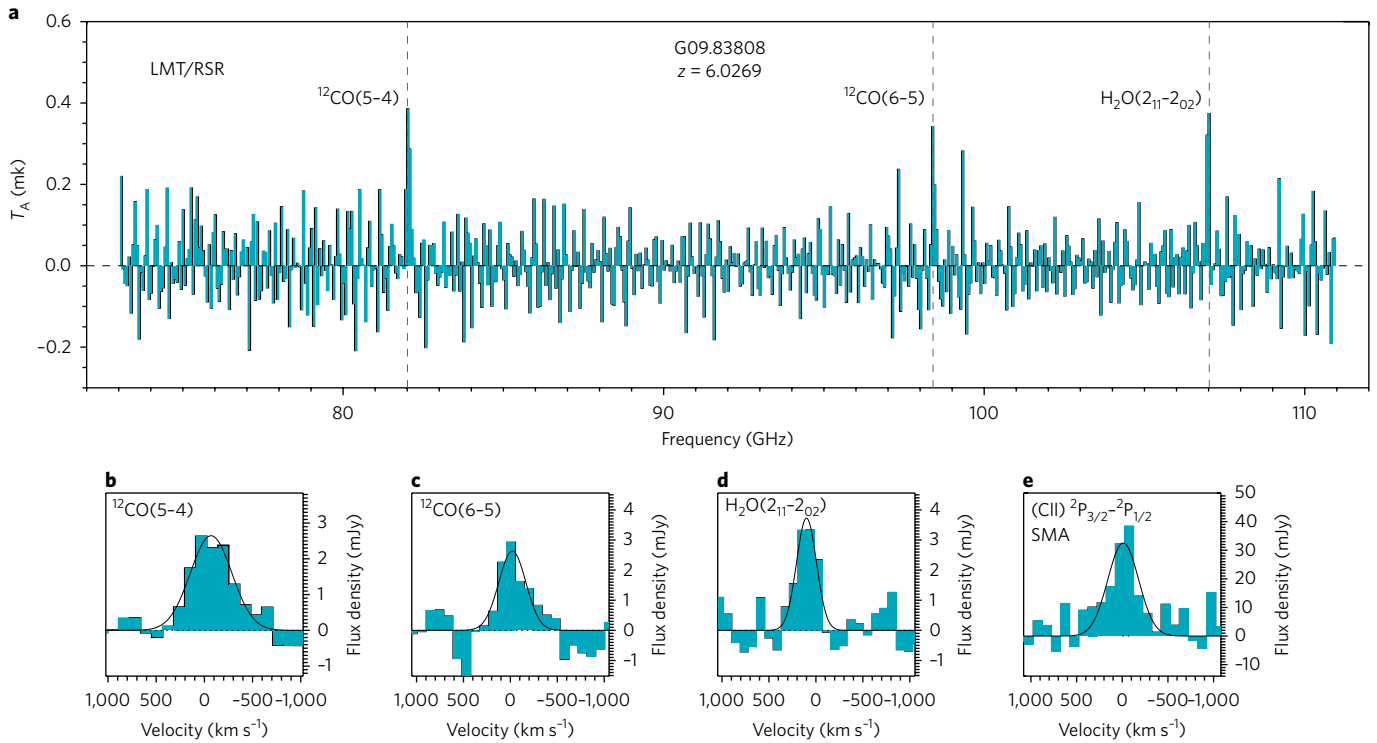


**Fig. 1 | Identification of molecular emission lines and redshift derivation.** **a**, Wide-band RSR 3 mm spectrum of G09 83808 taken with the LMT. The transitions detected above  $S/N=5$  are marked with vertical dashed lines and correspond to  $^{12}\text{CO}(5-4)$ ,  $^{12}\text{CO}(6-5)$  and  $\text{H}_2\text{O}(2_{11}-2_{02})$  at  $z = 6.0269 \pm 0.0006$ . The spectrum has been re-binned into two pixels bins ( $\sim 200 \text{ km s}^{-1}$ ) for better visualization. **b-d**, LMT/RSR unbinned spectra at the position of the detected lines, along with the best-fitting Gaussian profiles. **e**, SMA spectrum centred at the position of the detected line. The x axis is in velocity offset with respect to the derived redshift of  $z = 6.0269$ . The derived properties of the lines are reported in Table 1.

amplification factor of  $\mu = 9.3 \pm 1.0$ . This amplification factor was used to derive the intrinsic physical properties of G09 83808.

Using the Herschel 250, 350 and 500  $\mu\text{m}$  photometry<sup>14</sup> combined with the SCUBA-2 850  $\mu\text{m}$ <sup>14</sup> imaging and our AzTEC 1.1 mm observations (see Table 1), we modelled the continuum spectral energy distribution (SED; see Fig. 3). We estimated an infrared (8–1,000  $\mu\text{m}$ ) luminosity,  $L_{\text{IR}}$ , of  $3.8 \pm 0.5 \times 10^{12} L_{\odot}$  (corrected for gravitational magnification), which implies a dust-obscured star formation rate (SFR) of  $380 \pm 50 M_{\odot} \text{ yr}^{-1}$  (see Methods for more information). This means that G09 83808 is a member of the ultra luminous infrared galaxy (ULIRG)<sup>13</sup> population. This is one of the first submillimetre galaxies (SMGs) with an unambiguous spectroscopic redshift in this luminosity range at  $z > 5$ , lying between the extreme obscured starbursts<sup>6–12</sup> ( $> \sim 1,000 M_{\odot} \text{ yr}^{-1}$ ) discovered at submillimetre wavelengths and the ultraviolet/optical selected star-forming galaxies

with follow-up detections at submillimetre wavelengths<sup>16–18</sup> ( $< 100 M_{\odot} \text{ yr}^{-1}$ ). Within this luminosity range, only a handful of galaxies at  $z > 6$  are known, which were recently discovered around quasars<sup>19</sup> thanks to the serendipitous detection of a single emission line associated with [CII].

Although these galaxies are unreachable with the current generation of submillimetre wide-area surveys<sup>3,4</sup> without the benefit of gravitational amplification, they can be found in the deepest surveys recently achieved with ground-based telescopes, such as the James Clerk Maxwell Telescope SCUBA-2 Cosmology Legacy Survey. However, none of them has yet been spectroscopically confirmed. With the caveat of using the position of the dust SED peak as an estimation of redshift, a study based on SCUBA-2 Cosmology Legacy Survey observations<sup>5</sup> has derived a comoving space density of  $3.2 \times 10^{-6} \text{ Mpc}^{-3}$  for sources with  $300 < \text{SFR} < 1,000 M_{\odot} \text{ yr}^{-1}$  at

**Table 1 | Measured spectral line and continuum properties (not corrected for gravitational amplification)**

	Transition				Photometry <sup>a</sup>	
	$\text{CO}(5-4)$	$\text{CO}(6-5)$	$\text{H}_2\text{O}(2_{11}-2_{02})$	[CII]	[ $\mu\text{m}$ ]	[mJy]
$\nu_{\text{obs}}$ (GHz)	$82.031 \pm 0.007$	$98.41 \pm 0.01$	$106.993 \pm 0.007$	$270.35 \pm 0.03$	250	$9.7 \pm 5.4$
FWHM ( $\text{km s}^{-1}$ )	$490 \pm 60$	$320 \pm 70$	$240 \pm 40$	$400 \pm 70$	350	$24.6 \pm 7.9$
$S_{\text{int}}$ ( $\text{Jy km s}^{-1}$ )	$1.6 \pm 0.3$	$0.9 \pm 0.3$	$0.8 \pm 0.2$	$13.8 \pm 3.0$	500	$44.0 \pm 8.2$
$L'$ ( $10^{10} \text{ K km s}^{-1} \text{ pc}^{-2}$ )	$7.6 \pm 1.2$	$2.9 \pm 0.8$	$2.3 \pm 0.5$	$6.1 \pm 1.3$	850	$36.0 \pm 3.1$
					1,100	$20.0 \pm 1.0$

Photometric errors represent  $1\sigma$  uncertainties in the flux density measurements including calibration errors. The  $1\sigma$  uncertainties in the best-fitted Gaussian distribution parameters (central frequency, width and integrated flux density) are also reported and propagated to estimate the error in the line luminosity.<sup>a</sup>The flux densities at 250, 350, 500 and 850  $\mu\text{m}$  were taken from ref. <sup>14</sup>. FWHM, full width half maximum.

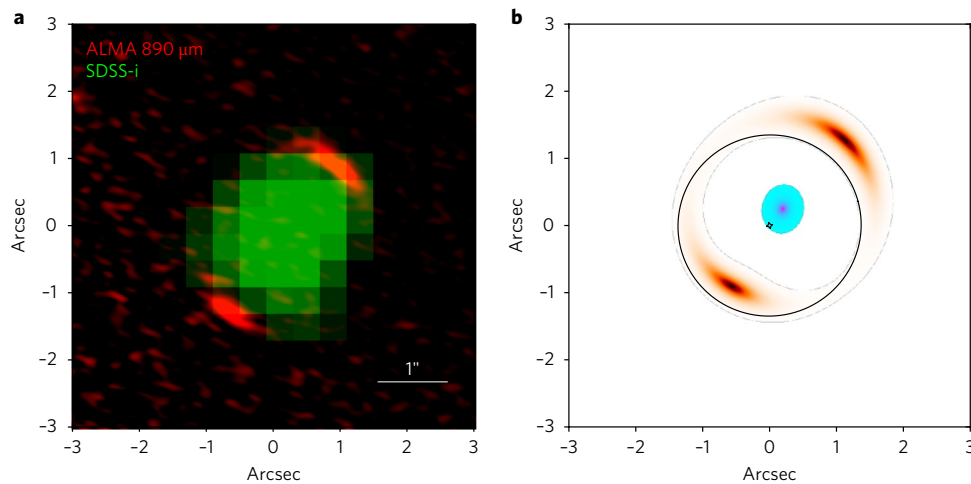


**Fig. 2 | ALMA high-angular resolution continuum observations and lensing model.** **a**, Colour composite image of G09 83808 centred at RA: 09 h 00 m 45.8 s, Dec: +00° 41' 23". The green channel represents the *i*-band data from the Sloan Digital Sky Survey and the red channel the ALMA 890  $\mu\text{m}$  observations. An Einstein ring-like structure of radius  $\approx 1.4$  arcsec in the ALMA image is clearly seen around a foreground galaxy at  $z = 0.776$ , which confirms that our high-redshift galaxy is strongly amplified. **b**, Best-fit lensing model based on the visibilities of ALMA observations, from which we derived a gravitational amplification of  $\mu = 9.3 \pm 1.0$ .

$5 < z \leq 6$  (that is, in the range probed by our galaxy). With a duty-cycle correction of  $\approx 40$  Myr, as the gas depletion time scale measured for G09 83808 (see below) and other galaxies<sup>11,20</sup>, we estimated the corrected comoving space density of this population of galaxies to be  $\approx 2 \times 10^{-5} \text{ Mpc}^{-3}$ , which perfectly matches that of massive quiescent galaxies at  $z \approx 3-4$  (refs<sup>21,22</sup>). This suggests that these ULIRG-type galaxies at  $5 \leq z \leq 6$  are the progenitors of these quiescent galaxies, which cannot be explained only by the rare extreme starburst (like HFLS3), since they are an order of magnitude less abundant<sup>14</sup>.

Based on the CO lines detected in the LMT/RSR spectrum, we derived a molecular gas mass of  $M(\text{H}_2) = 1.6 \pm 0.6 \times 10^{10} M_\odot$  (see Methods for details). This implies a gas depletion timescale of  $M(\text{H}_2)/\text{SFR} \approx 40$  Myr, consistent with the value found for other SMGs at lower redshifts with ULIRG luminosity<sup>23</sup>. G09 83808 shows a remarkable large gas mass fraction of  $f_{\text{gas}} = M_{\text{H}_2} / M_{\text{dyn}} \sim 60\%$  (see Methods), which is among the largest measured for star forming galaxies at  $z \approx 2-3$  (ref.<sup>24</sup>). The CO(6-5)/CO(5-4) line luminosity ratio of  $0.4 \pm 0.1$  is in agreement with local ULIRGs (although lower than the average<sup>25</sup>) and implies a CO ladder peaking at  $J \leq 5$  (that is, less excited than active galactic nucleus-dominated galaxies<sup>26</sup>). These two CO transitions, as well as the  $\text{H}_2\text{O}$  line, lie (within the error bars) on their respective FIR/infrared line luminosity relations ( $L_{\text{FIR}} \propto L_{\text{CO}(6-5)}^{0.93}$ ,  $L_{\text{FIR}} \propto L_{\text{CO}(5-4)}^{0.97}$  and  $L_{\text{H}_2\text{O}} \propto L_{\text{IR}}^{1.16}$ ) found for local ULIRGs and lower redshifts SMGs<sup>25,27</sup>. The star-formation efficiency of our galaxy, estimated through the  $L'_{\text{CO}}-L_{\text{IR}}$  relation (which describes the relationship between the luminosity due to star formation and the gas content), is similar to local (U)LIRGs (see Fig. 4). The same star-formation efficiency can be found across several decades of molecular gas masses from  $z = 6$  to  $z \sim 0$  (that is, during the past 12.8 Gyr of the Universe). In addition, the estimated dust mass of  $M_{\text{d}} = 1.9 \pm 0.4 \times 10^8 M_\odot$  results in a gas-to-dust ratio,  $\delta_{\text{GDR}}$ , of  $80 \pm 30$ . This is in agreement with the value estimated for HFLS3<sup>11</sup> and also with local (U)LIRGs<sup>28</sup> ( $\delta_{\text{GDR}} = 120 \pm 28$ ).

The luminosity of the [CII] ionized carbon line detected with the SMA is  $1.3 \pm 0.4 \times 10^9 L_\odot$ , which corresponds to a [CII]/FIR ratio of  $3.4 \pm 1.1 \times 10^{-4}$ , a value that is among the lowest measured for local (U)LIRGs and SMGs. As shown in Fig. 4, our source follows the same [CII] deficiency trend measured for local LIRGs<sup>29</sup> extending it to  $L_{\text{FIR}} \sim 10^{12} L_\odot$  and up to  $z = 6$ . The [CII]/FIR ratio of G09 83808 is also consistent with the lowest values measured for lower-redshift

SMGs and lies on a region where SMGs and active galactic nucleus host galaxies converge (Fig. 4). It may be the case that other SMGs suffer from gravitational amplification, which could help reduce the large scatter since many of these galaxies should fall along the LIRG relation when corrected for magnification. However, the intrinsic scatter in the relation is high<sup>29</sup>, even for the local sample, and therefore, larger samples of SMGs are required to derive conclusions about the origin of the [CII] deficiency.

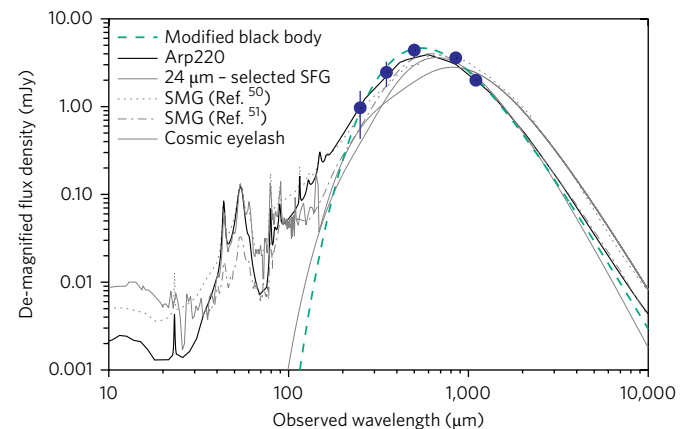


**Fig. 3 | Photometry and SED.** De-magnified (with  $\mu = 9.3 \pm 1.0$ ) flux densities at 250, 350, 500, 850 and 1,100  $\mu\text{m}$  from Herschel/Spectral and Photometric Imaging Receiver, James Clerk Maxwell Telescope/SCUBA-2 and LMT/AzTEC are indicated by the blue circles, with bars representing the photometric  $1\sigma$  errors including calibration and lensing model uncertainties. These flux densities were fitted with different SED templates, including: Arp220, Cosmic Eyelash, two average SMG templates, an average 24  $\mu\text{m}$  selected star-forming galaxy template and a modified black body (see Methods for details). We achieved the lowest  $\chi^2$  with the Arp220 template, from which we derived an infrared luminosity of  $3.8 \pm 0.5 \times 10^{12} L_\odot$  (corrected for magnification). From the best-fit modified black body distribution, we derived a dust temperature of  $49 \pm 3$  K. As discussed in the Methods, the CMB effects were not significant. SFG, star-forming galaxy.

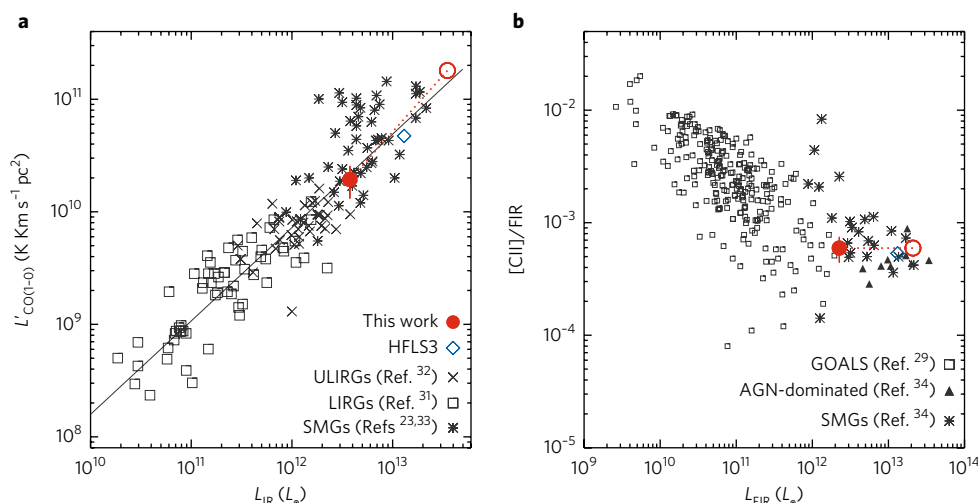


**Fig. 4 | Star formation efficiency and [CII] deficiency.** **a**, Lens-corrected CO(1-0) luminosity versus infrared luminosity ( $L_{\text{CO}(1-0)}-L_{\text{IR}}$ ) as a proxy for the star-formation efficiency of G09 83808. For comparison, local LIRGs<sup>31</sup>, ULIRGs<sup>32</sup> and lower-redshift SMGs<sup>23,33</sup> are plotted along with the best-fit relation to the three samples<sup>23</sup>. As can be seen, G09 83808 falls on the same relation (as well as HFLS3<sup>11</sup> after correcting for magnification<sup>15</sup>), which suggests that the same star formation efficiency holds from  $z=0$  to  $z=6$  (that is, during the past  $\sim 12.8$  Gyr). The empty circle represents the position of our source if no lensing amplification correction is applied. **b**, [CII]/FIR versus de-magnified (filled circle) and amplified (empty circle) FIR luminosity for G09 83808. For comparison, we also plot a sample of (U)LIRG galaxies from the Great Observatories All-sky Survey (GOALS)<sup>29</sup> and a compilation of high-redshift sources<sup>34</sup> that includes SMGs and active galactic nucleus-dominated sources. As can be seen, our source follows the same trend as that found for local (U)LIRGs once corrected for magnification.

We confirm the existence of ULIRG-like galaxies within the first billion years of the Universe's history. These sources may be more representative of the dusty star-forming galaxy population at these epochs than the extreme starbursts previously discovered. Four emission-line-selected galaxies with similar luminosities and redshifts have been found recently around quasars<sup>19</sup> (with the caveat of using just one line for redshift determination); however, the properties of these sources may be affected by the companion quasar and therefore may not be representative of the whole population. Although G09 83808 shows similar properties to those measured in lower-redshift SMGs, its higher dust temperature ( $T_d = 49 \pm 3$  K) and compact morphology ( $R_{1/2} = 0.6 \pm 0.1$  kpc) resemble local ULIRGs. For comparison, typical ultraviolet/optically selected star-forming galaxies at  $z \sim 6$  have SFRs  $\sim 10$  times lower and radii  $\sim 1.7$  times larger than G09 83808 (ref. 30). This study is hence crucial for understanding the evolutionary path of SMGs and their link with local galaxies. Although a larger sample is needed to statistically estimate the properties of these sources and their contribution to the cosmic star formation history, this galaxy suggests that star formation in dusty star-forming galaxies has been driven by similar physical processes during the past  $\sim 12.8$  Gyr.

## Methods

**Observations and data reduction.** *LMT observations.* Continuum and spectroscopic observations were obtained using the LMT<sup>35</sup> (principal investigator: D.H.H.), located on the summit of Volcán Sierra Negra (Tliltépetl), Mexico, at  $\sim 4,600$  m above sea level. Observations were carried out during the Early Science phase of the telescope using the 1.1 mm continuum camera AzTEC<sup>36</sup> and the 3 mm spectrograph RSR<sup>37</sup>. During these observations, only the inner 32-m-diameter region of the telescope active surface was illuminated, which provided an effective beam size of  $\approx 8.5$  arcsec at 1.1 mm and between 20 and 28 arcsec in the RSR 3 mm window (75–110 GHz).

AzTEC observations were performed on 2014 November 10 with an opacity of  $\tau_{225} = 0.07$  and a total on-source integration time of 11 min. Data reduction was done following the AzTEC standard pipeline<sup>38</sup>. G09 83808 was detected with a  $S/N \approx 20$  with a flux density of  $S_{1.1\text{mm}} = 20.0 \pm 1.0$  mJy. RSR observations were subsequently taken at the AzTEC position during two different periods: February 2016 and February 2017, on five different nights with an opacity range of  $\tau_{225} = 0.05-0.15$  and a total integration time of 8 h. Pointing observations on bright millimetre sources were performed every hour. Data reduction was performed

using the Data Reduction and Analysis Methods in Python. The final spectra were obtained by averaging all scans using  $1/\sigma^2$  weights after flagging bad data. Finally, to convert from antenna temperature units to flux, a factor of  $7 \text{ Jy K}^{-1}$  was used<sup>39</sup>. The final spectrum shows three lines detected at  $S/N > 5$  associated with CO(6–5), CO(5–4) and  $\text{H}_2\text{O}(2_{11}-2_{02})$  at  $z = 6.0269$ . A cross-correlation template analysis<sup>39</sup> also identified this redshift as the best solution with a  $S/N = 9.1$ . Figure 1 shows the final spectrum after a Savitzky–Golay filter<sup>40</sup> was applied for better visualization (the filter does not modify any of the properties of the detected lines).

At the redshift of our source, the [CII] 158  $\mu\text{m}$  line (see below) falls within the AzTEC band pass and then contributes to the total flux density measured at 1.1 mm. However, the contamination from the line is measured to be less than 2%. Even if the [CII] line luminosity were as high as 1% of the total infrared luminosity, the contamination to the AzTEC measurement would only be  $\sim 6\%$ , which is similar to the absolute flux calibration uncertainty. Therefore, and at least for this source, the contamination of the emission line to the 1.1 mm continuum flux density is less important than anticipated<sup>41</sup>.

*SMA observations.* G09 83808 was observed with the SMA (principal investigator: J.A.Z.) on Mauna Kea, Hawaii, on 2017 April 03. The weather conditions were good, with an average atmospheric opacity of  $\tau_{225} = 0.07$  and stable phase. The seven available array antennas were in a compact configuration that provided baseline lengths from 8 to 77 m. The '345' receiver set was tuned to provide spectral coverage  $\pm(4-12)$  GHz from a local oscillator frequency of 277.5 GHz, specifically to span a broad range around the estimated (redshifted) [CII] line frequency of  $\sim 270.5$  GHz in the lower sideband. The SMA Wideband Astronomical ROACH2 Machine correlator provided uniform channel spacing of 140 kHz ( $\sim 0.16 \text{ km s}^{-1}$ ) over the full bandwidth. The usable field of view was set by the full width half maximum primary beam size of  $\sim 47$  arcsec at this frequency.

The basic observing sequence consisted of a loop of 2 min each on the gain calibrators J0909+013 (1.57 Jy) and J0831+044 (0.47 Jy) and 17.5 min on G09 83808. The track spanned an hour angle range of  $-0.8$  to  $4.8$  for the target source. Passband calibration was obtained with observations of the strong quasar 3C279. The absolute flux scale was set using observations of Callisto, with an estimated accuracy of 20%. All of the basic calibration steps were performed using standard procedures in the MIR software package (version 170227; [www.cfa.harvard.edu/~cqi/mircook.html](http://www.cfa.harvard.edu/~cqi/mircook.html)). The calibrated visibilities were exported to the MIRIAD software package for imaging and deconvolution<sup>42</sup>. Within MIRIAD, the task 'uvaver' was used to combine the four correlator windows of the lower sideband and to resample the visibilities to  $50 \text{ km s}^{-1}$  spectral resolution. The task 'uvlin' was used for continuum subtraction, using a linear fit to line-free channel ranges in the band. The task 'invert' provided Fourier inversion for both continuum and spectral line imaging, followed by 'clean' for deconvolution. The synthesized beam size obtained with natural weighting was  $2.5'' \times 2.3''$ , p.a.  $82^\circ$  for the spectral line data cube, with rms noise  $7.1$  mJy per  $50 \text{ km s}^{-1}$  bin. The final spectrum (see Fig. 1)

was then extracted from a rectangular region that comprised all the continuum emission. We measured the continuum flux density of the source to be  $21.5 \pm 3$  mJy, which was in very good agreement with the AzTEC photometry.

**ALMA observations.** The ALMA high-resolution 870  $\mu\text{m}$  observations used in this work were taken on 2015 August 31 (project 2013.1.00001.S; principal investigator: R.J.I.; ref. <sup>49</sup>) when the array was in a relatively extended configuration with baselines up to 1.6 km. The default continuum spectral configuration was used, covering (335.49–339.49) GHz and (347.49–351.49) GHz. The data were calibrated using the ALMA pipeline, with no further manual flagging required. The calibrated visibilities were imaged using Briggs weighting with robust = 0.5, which is a good compromise between sensitivity and angular resolution. The beam size was then  $\sim 0.12''$  and the continuum sensitivity was  $\sim$  r.m.s.  $\sim 0.1$  mJy beam<sup>-1</sup>. The visibility weighting in ALMA data is generally only correct in a relative sense, while our subsequent lens modelling procedure (see 'Lensing Model' below) requires an absolute estimate of the noise in the data. The data weights are determined by differencing successive visibilities on the same baseline, polarization and frequency baseband. The ALMA data also serendipitously cover the frequency of the redshifted 122  $\mu\text{m}$  [N<sub>II</sub>] line; this line is not detected at  $>3\sigma$  significance.

**Lensing model.** The lens model was created using the publicly available 'visilens' code<sup>44</sup>. Briefly, the lens mass profile was parameterized as a singular isothermal ellipsoid and the background source was modelled with a single elliptical Sérsic profile. The parameter space was explored using a Markov chain Monte Carlo sampling method, generating a model lensed image at each proposed combination of lens and source parameters. The redshifts of the lens and background sources were fixed at  $z = 0.776$  (based on X-Shooter/VLT observations<sup>45</sup>) and  $z = 6.027$ , respectively. As pixel values in interferometric images are correlated and subject to difficult-to-model residual calibration errors, the proposed model image was inverted to the visibility domain and sampled at the  $uv$  coordinates of the ALMA data. We also allowed for residual antenna-based phase calibration errors in the model, which could be due to, for example, uncompensated atmospheric delays. The phase shifts of all antennas were  $<10$  deg, indicating that no significant antenna-based calibration problems remained.

The lensed emission was reasonably well fit by a single background Sérsic component, leaving peak residuals of  $\sim 4\sigma$  (the source was detected at peak significance  $\sim 20\sigma$ ). These residuals may indicate that either the lens, source or both are more complex than the simple parametric forms we assumed. We have verified that an additional background source component is not statistically motivated. The best-fit magnification of the source is  $\mu_{890\mu\text{m}} = 9.3 \pm 1.0$ , with an intrinsic flux density  $S_{890\mu\text{m}} = 4.3 \pm 0.5$  mJy and a half-light radius of  $0.10 \pm 0.01''$  ( $= 0.6 \pm 0.1$  kpc). This compact morphology resembles the sizes found for local ULIRGs<sup>46</sup> ( $\sim 0.5$  kpc), which are smaller than the typical values in SMGs ( $\sim 1.8$  kpc; ref. <sup>47</sup>).

**SED fitting and dust properties.** We fit different galaxy SED templates to the photometry of G09 83808 through a  $\chi^2$  minimization method. We included the SED template of Arp220 (ref. <sup>48</sup>), Cosmic Eyelash<sup>49</sup> (SMM J2135-0102), two average SMGs templates<sup>50,51</sup> and, finally, a composite SED of a 24  $\mu\text{m}$  selected star-forming galaxy<sup>52</sup>. All the SED templates were fixed at  $z = 6.027$ . The Arp220 SED template gave us the best fit with  $\chi^2_{\text{red}} = 0.7$ . Using this template, we derived an infrared (8–1,000  $\mu\text{m}$ ) luminosity of  $3.8 \pm 0.5 \times 10^{12} L_{\odot}$  and a FIR (42.5–122.5  $\mu\text{m}$ ) luminosity of  $2.3 \pm 0.3 \times 10^{12} L_{\odot}$  (both corrected for gravitational amplification).

For comparison, if we adopt instead an SMGs average template ( $\chi^2_{\text{red}} = 1.2$ ), we obtain  $L_{\text{IR}} = 3.0 \pm 0.4 \times 10^{12} L_{\odot}$ , which is in good agreement with the value derived using the Arp220 template. Using Kennicutt standard relation<sup>53</sup> for a Chabrier initial mass function<sup>54</sup>, this infrared luminosity corresponds to an SFR of  $380 \pm 50 M_{\odot} \text{ yr}^{-1}$ , or to  $570 \pm 70 M_{\odot} \text{ yr}^{-1}$  if the most recent relation<sup>55</sup> is used. If we adopt instead the Kennicutt calibration<sup>53</sup> for a Salpeter initial mass function<sup>56</sup>, the SFR increases to  $640 \pm 90 M_{\odot} \text{ yr}^{-1}$ , which is still below the range probed by other SMGs at  $z \sim 5$ .

We also use a modified blackbody function to fit our photometric measurements described by

$$S_{\nu} \propto [1 - \exp\{-\nu/\nu_0\}^{\beta}] B(\nu, T_d) \quad (1)$$

where  $S_{\nu}$  is the flux density at frequency  $\nu$ ,  $\nu_0$  is the rest-frame frequency at which the emission becomes optically thick,  $T_d$  is the dust temperature,  $\beta$  is the emissivity index and  $B(\nu, T_d)$  is the Planck function at temperature  $T_d$ . To minimize the number of free parameters, the emissivity index is fixed (previous observational works suggest  $\beta = 1.5$ – $2$ ; refs <sup>57–59</sup>), as well as  $\nu_0 = c/100 \mu\text{m}$  (refs <sup>11,60</sup>), where  $c$  is the speed of light. From the best fit ( $\chi^2 \approx 1.1$ ), we derive  $T_d = 49 \pm 3$  K for  $\beta = 1.8$  and  $T_d = 52 \pm 3$  K for  $\beta = 1.5$ . For these dust temperatures and at the redshift of our source, the CMB effects<sup>61</sup> are not significant ( $\Delta T < \sim 1$  K).

Assuming the dust is isothermal, the dust mass,  $M_d$ , is estimated from

$$M_d = \frac{S_{\nu/(1+z)} D_L^2}{(1+z) \kappa_{\nu} B(\nu, T_d)} \quad (2)$$

where  $S_{\nu}$  is the flux density at frequency  $\nu$ ,  $\kappa_{\nu}$  is the dust mass absorption coefficient at  $\nu$ ,  $T_d$  is the dust temperature,  $D_L$  is the luminosity distance in Mpc and  $B(\nu, T_d)$  is the

Planck function at temperature  $T_d$ . The dust mass absorption follows the same power law as the optical depth,  $\kappa \propto \nu^{\beta}$ . Assuming normalization of  $\kappa_d$  ( $850 \mu\text{m}$ )  $= 0.07 \text{ m}^2 \text{ kg}^{-1}$  (ref. <sup>62</sup>) and a dust temperature of  $49 \pm 3$  K, we estimate a dust mass of  $M_d = 1.9 \pm 0.4 \times 10^8 M_{\odot}$  after correcting for the CMB effects<sup>61</sup> (although this correction is less than 5%). These calculations do not include the uncertainties of the dust mass absorption coefficient, which could be at least a factor of 3 (ref. <sup>63</sup>). If we use instead a lower dust temperature of 35 K, the dust mass increases by a factor of  $\sim 2$ .

We also fit the observed photometry with the MAGPHYS<sup>64</sup> SED modelling code and found consistent results within the error bars, with median values of  $\text{SFR} = 360_{-70}^{+80} M_{\odot} \text{ yr}^{-1}$ ,  $L_{\text{IR}} = 4.5 \pm 0.7 \times 10^{12} L_{\odot}$ ,  $T_d = 40_{-2}^{+4}$  K and  $M_d = 4.2 \pm 0.7 \times 10^8 M_{\odot}$ .

**Spectral line properties.** We calculated the line luminosity for each detected line following the standard relation<sup>65</sup> described by:

$$L'_{\text{CO}} = 3.25 \times 10^7 S_{\text{CO}} \Delta V \nu_{\text{obs}}^{-2} D_L^2 (1+z)^{-3} \quad (3)$$

where  $L'_{\text{CO}}$  is the line luminosity in  $\text{K km s}^{-1} \text{ pc}^2$ ,  $S_{\text{CO}} \Delta V$  is the velocity-integrated line flux in  $\text{Jy km s}^{-1}$  and  $\nu_{\text{obs}}$  is the observed central frequency of the line in GHz. The integrated flux,  $S_{\text{CO}} \Delta V$ , is calculated as the integral of the best-fit Gaussian distribution and its associated uncertainty through Monte Carlo simulations taking into account the errors in the Gaussian parameters (that is, peak flux density and line width). To estimate the line luminosity in  $L_{\odot}$ , we used  $L = 3 \times 10^{-11} \nu_r^3 L'$ , where  $\nu_r$  is the rest frequency of the line<sup>65</sup>. All properties are summarized in Table 1.

**CO(1–0) line luminosity and molecular gas mass.** The molecular gas mass,  $M(\text{H}_2)$ , can be derived using the CO luminosity to molecular gas mass conversion factor,  $\alpha$ , following the relation

$$M(\text{H}_2) = \alpha L'_{\text{CO}(1-0)} \quad (4)$$

For the  $L'_{\text{CO}(1-0)}$  line luminosity, we adopted the average value of  $L'_{\text{CO}(1-0)} = 2.0 \pm 0.8 \times 10^{10} \text{ K km s}^{-1} \text{ pc}^2$  extrapolated from our CO(6–5) and CO(5–4) transitions and correcting for gravitational amplification. The extrapolation was done using average brightness ratios found for lower-redshift SMGs<sup>23</sup> ( $L'_{\text{CO}(5-4)}/L'_{\text{CO}(1-0)} = 0.32 \pm 0.05$ ,  $L'_{\text{CO}(6-5)}/L'_{\text{CO}(1-0)} = 0.21 \pm 0.04$ ). This sample includes galaxies with similar luminosities to G09 83808 and is in agreement with those found for local ULIRGs<sup>25</sup> (within the large scatter). In contrast, if we use the relationship between the Rayleigh–Jeans specific luminosity and CO(1–0) luminosity<sup>66</sup>,  $L'_{\text{CO}(1-0)}$  ( $\text{K km s}^{-1} \text{ pc}^2$ )  $= 3.02 \times 10^{-21} L_{\nu}$  ( $\text{erg s}^{-1} \text{ Hz}^{-1}$ ), we obtain a consistent line luminosity of  $1 \pm 0.1 \times 10^{10} \text{ K km s}^{-1} \text{ pc}^2$  (assuming a mass-weighted dust temperature of 35 K, which is different from the luminosity-weighted dust temperature determined from the SED fitting<sup>66</sup>). Using the former value and  $\alpha = 0.8 M_{\odot} (\text{K km s}^{-1} \text{ pc}^2)^{-1}$ , which is appropriate for starburst galaxies<sup>66</sup> (although some studies suggest larger values<sup>67</sup>), we derive a molecular mass of  $M(\text{H}_2) = 1.6 \pm 0.6 \times 10^{10} M_{\odot}$ .

**Dynamical mass and gas mass fraction.** Dynamical mass was derived using the 'isotropic virial estimator', which has been shown to be appropriate for lower-redshift SMGs<sup>68</sup>:

$$M_{\text{dyn}}(M_{\odot}) = 2.8 \times 10^5 \Delta \nu_{\text{FWHM}}^2 (\text{km s}^{-1}) R_{1/2} (\text{kpc}) \quad (5)$$

where  $\Delta \nu_{\text{FWHM}}$  is the integrated line full width half maximum, which was assumed to be  $400 \text{ km s}^{-1}$  (as the average between the CO and [CII] lines) and  $R_{1/2}$  is the half-light radius of  $\sim 0.6$  kpc (derived from the lensing model of the continuum emission). This results in a dynamical mass of  $M_{\text{dyn}} = 2.6 \times 10^{10} M_{\odot}$ . Using this estimation, we calculate a gas mass fraction of  $f_{\text{gas}} = M_{\text{H}_2} / M_{\text{dyn}} \approx 60\%$ . This constrains the CO-luminosity-to-molecular-gas-mass conversion factor to  $\alpha < \sim 1.4 M_{\odot} (\text{K km s}^{-1} \text{ pc}^2)^{-1}$ , otherwise the molecular gas mass would exceed the dynamical mass.

**Data availability.** The datasets generated and analysed during this study are available from the corresponding author on reasonable request. The ALMA observations presented here are part of the project 2013.1.00001.S and the SMA data correspond to the project 2016B-S078.

Received: 27 July 2017; Accepted: 28 September 2017;  
Published online: 6 November 2017

## References

1. Smail, I., Ivison, R. J. & Blain, A. W. A deep sub-millimeter survey of lensing clusters: a new window on galaxy formation and evolution. *Astrophys. J. Lett.* **490**, L5–L8 (1997).
2. Hughes, D. et al. High-redshift star formation in the Hubble Deep Field revealed by a submillimetre-wavelength survey. *Nature* **394**, 241–247 (1998).
3. Oliver, S. et al. The Herschel Multi-tiered Extragalactic Survey: HerMES. *Mon. Not. R. Astron. Soc.* **424**, 1614–1635 (2012).

4. Valiante, E. et al. The Herschel-ATLAS data release 1 – I. Maps, catalogues and number counts. *Mon. Not. R. Astron. Soc.* **462**, 3146–3179 (2016).
5. Michałowski, M. et al. The SCUBA-2 Cosmology Legacy Survey: the nature of bright submm galaxies from 2 deg<sup>2</sup> of 850- $\mu$ m imaging. *Mon. Not. R. Astron. Soc.* **469**, 492–515 (2017).
6. Capak, P. et al. A massive protocluster of galaxies at a redshift of  $z \approx 5.3$ . *Nature* **470**, 233–235 (2011).
7. Combes, F. et al. A bright  $z=5.2$  lensed submillimeter galaxy in the field of Abell 773. *HLSJ091828.6+514223*. *Astron. Astrophys. Lett.* **538**, L4 (2012).
8. Walter, F. et al. The intense starburst HDF850.1 in a galaxy overdensity at  $z \approx 5.2$  in the Hubble Deep Field. *Nature* **486**, 233–236 (2012).
9. Ma, J. et al. Stellar masses and star formation rates of lensed, dusty, star-forming galaxies from the SPT survey. *Astrophys. J.* **812**, 88–104 (2015).
10. Riechers, D. et al. Rise of the titans: a dusty, hyper-luminous '870 micron riser' galaxy at  $z \sim 6$ . Preprint at <https://arxiv.org/abs/1705.09660> (2017).
11. Riechers, D. et al. A dust-obscured massive maximum-starburst galaxy at a redshift of 6.34. *Nature* **496**, 329–333 (2013).
12. Strandet, M. et al. ISM properties of a massive dusty star-forming galaxy discovered at  $z \sim 7$ . *Astrophys. J. Lett.* **842**, L15 (2017).
13. Sanders, D. & Mirabel, I. Luminous infrared galaxies. *Ann. Rev. Astron. Astrophys.* **34**, 749–792 (1996).
14. Ivison, R. et al. The space density of luminous dusty star-forming galaxies at  $z > 4$ : SCUBA-2 and LABOCA imaging of ultrared galaxies from Herschel-ATLAS. *Astrophys. J.* **832**, 78 (2016).
15. Cooray, A. et al. HerMES: the rest-frame UV emission and a lensing model for the  $z=6.34$  luminous dusty starburst galaxy HFLS3. *Astrophys. J.* **790**, 40–50 (2014).
16. Capak, P. et al. Galaxies at redshifts 5 to 6 with systematically low dust content and high [C II] emission. *Nature* **522**, 455–458 (2015).
17. Watson, D. et al. A dusty, normal galaxy in the epoch of reionization. *Nature* **519**, 327–330 (2015).
18. Willott, C., Carilli, C., Wagg, J. & Wang, R. Star formation and the interstellar medium in  $z > 6$  UV-luminous Lyman-break galaxies. *Astrophys. J.* **807**, 180–188 (2015).
19. Decarli, R. et al. Rapidly star-forming galaxies adjacent to quasars at redshifts exceeding 6. *Nature* **545**, 457–461 (2017).
20. Oteo, I. et al. Witnessing the birth of the red sequence: ALMA high-resolution imaging of [C II] and dust in two interacting ultra-red starbursts at  $z=4.425$ . *Astrophys. J.* **827**, 34 (2016).
21. Nayyeri, H. et al. A study of massive and evolved galaxies at high redshift. *Astrophys. J.* **794**, 68 (2014).
22. Straatman, C. et al. The sizes of massive quiescent and star-forming galaxies at  $z \sim 4$  with ZFOURGE and CANDELS. *Astrophys. J. Lett.* **808**, L29 (2015).
23. Bothwell, M. et al. A survey of molecular gas in luminous sub-millimetre galaxies. *Mon. Not. R. Astron. Soc.* **429**, 3047–3067 (2013).
24. Tacconi, L. et al. High molecular gas fractions in normal massive star forming galaxies in the young Universe. *Nature* **463**, 781–784 (2010).
25. Greve, T. et al. Star formation relations and CO spectral line energy distributions across the J-ladder and redshift. *Astrophys. J.* **794**, 142 (2014).
26. Carilli, C. & Walter, F. Cool gas in high-redshift galaxies. *Ann. Rev. Astron. Astrophys.* **51**, 105–161 (2013).
27. Yang, C. et al. Submillimeter H<sub>2</sub>O and H<sub>2</sub>O<sup>+</sup> emission in lensed ultra- and hyper-luminous infrared galaxies at  $z=2-4$ . *Astron. Astrophys.* **595**, 80 (2016).
28. Wilson, C. et al. Luminous infrared galaxies with the submillimeter array. I. Survey overview and the central gas to dust ratio. *Astrophys. J. Suppl. Ser.* **178**, 189–224 (2008).
29. Daz-Santos, T. et al. Explaining the [C II]157.7  $\mu$ m deficit in luminous infrared galaxies—first results from a Herschel/PACS study of the GOALS sample. *Astrophys. J.* **774**, 68 (2013).
30. Rodriguez-Puebla, A., Primack, J., Avila-Reese, V. & Faber, S. Constraining the galaxy-halo connection over the last 13.3 Gyr: star formation histories, galaxy mergers and structural properties. *Mon. Not. R. Astron. Soc.* **470**, 651–687 (2017).
31. Sanders, D., Scoville, N. & Soifer, B. Molecular gas in luminous infrared galaxies. *Astrophys. J.* **370**, 158–171 (1991).
32. Solomon, P., Downes, D., Radford, S. J. E. & Barrett, J. W. The molecular interstellar medium in ultraluminous infrared galaxies. *Astrophys. J.* **478**, 144–161 (1997).
33. Aravena, M. et al. A survey of the cold molecular gas in gravitationally lensed star-forming galaxies at  $z > 2$ . *Mon. Not. R. Astron. Soc.* **457**, 4406–4420 (2016).
34. Gullberg, B. et al. The nature of the [C II] emission in dusty star-forming galaxies from the SPT survey. *Mon. Not. R. Astron. Soc.* **449**, 2883–2900 (2015).
35. Hughes, D. et al. The Large Millimeter Telescope. *Proc. SPIE* **7733**, 13 (2010).
36. Wilson, G. et al. The AzTEC mm-wavelength camera. *Mon. Not. R. Astron. Soc.* **386**, 807–818 (2008).
37. Erickson, N. et al. An ultra-wideband receiver and spectrometer for 74–110 GHz. *ASPCS* **375**, 71 (2007).
38. Scott, K. B. et al. AzTEC millimetre survey of the COSMOS field – I. Data reduction and source catalogue. *Mon. Not. R. Astron. Soc.* **385**, 12225–2238 (2008).
39. Yun, M. S. et al. Early science with the Large Millimeter Telescope: CO and [C II] emission in the  $z=4.3$  AzTEC J095942.9+022938 (COSMOS AzTEC-1). *Mon. Not. R. Astron. Soc.* **454**, 3485–3499 (2015).
40. Savitzky, A. & Golay, M. J. E. Smoothing and differentiation of data by simplified least squares procedures. *Anal. Chem.* **36**, 1627–1639 (1964).
41. Smail, I., Swinbank, A. M., Ivison, R. J. & Ibar, E. The potential influence of far-infrared emission lines on the selection of high-redshift galaxies. *Mon. Not. R. Astron. Soc. Lett.* **414**, L95–L99 (2011).
42. Sault, R. J., Teuben, P. J. & Wright, M. C. H. A retrospective view of Miriad. in *Astronomical Data Analysis Software and Systems IV* (eds Shaw, R., Payne, H. E. & Hayes, J. J. E.) *ASP Conf. Series* **77**, 433–436 (1995).
43. Oteo, I. et al. Witnessing the birth of the red sequence: the physical scale and morphology of dust emission in hyper-luminous starbursts in the early Universe. Preprint at <https://arxiv.org/abs/1709.04191> (2017).
44. Spilker, J. et al. ALMA imaging and gravitational lens models of South Pole Telescope—selected dusty, star-forming galaxies at high redshifts. *Astrophys. J.* **826**, 112 (2016).
45. Fudamoto, Y. et al. The most distant, luminous, dusty star-forming galaxies: redshifts from NOEMA and ALMA spectral scans. *Mon. Not. R. Astron. Soc.* **472**, 2028–2041 (2017).
46. Lutz, D. et al. The far-infrared emitting region in local galaxies and QSOs: size and scaling relations. *Astron. Astrophys.* **591**, 136 (2016).
47. Hodge, J. et al. Kiloparsec-scale dust disks in high-redshift luminous submillimeter galaxies. *Astrophys. J.* **833**, 103 (2016).
48. Silva, L., Granato, G. L., Bressan, A. & Danese, L. Modeling the effects of dust on galactic spectral energy distributions from the ultraviolet to the millimeter band. *Astrophys. J.* **509**, 103–117 (1998).
49. Ivison, R. et al. Herschel and SCUBA-2 imaging and spectroscopy of a bright, lensed submillimetre galaxy at  $z=2.3$ . *Astron. Astrophys. Lett.* **518**, L35 (2010).
50. Michałowski, M. J., Hjorth, J. & Watson, D. Cosmic evolution of submillimeter galaxies and their contribution to stellar mass assembly. *Astron. Astrophys.* **514**, A67 (2010).
51. Pope, A. et al. Mid-infrared spectral diagnosis of submillimeter galaxies. *Astrophys. J.* **675**, 1171–1193 (2008).
52. Kirkpatrick, A. et al. GOODS-Herschel: impact of active galactic nuclei and star formation activity on infrared spectral energy distributions at high redshift. *Astrophys. J.* **759**, 139 (2012).
53. Kennicutt, R. C. Jr The global Schmidt law in star-forming galaxies. *Astrophys. J.* **498**, 541–552 (1998).
54. Chabrier, G. The galactic disk mass function: reconciliation of the Hubble Space Telescope and nearby determinations. *Astrophys. J.* **586**, L133–L136 (2003).
55. Kennicutt, R. & Evans, N. Star formation in the Milky Way and nearby galaxies. *Ann. Rev. Astron. Astrophys.* **50**, 531–608 (2012).
56. Salpeter, E. The luminosity function and stellar evolution. *Astrophys. J.* **121**, 161 (1955).
57. Dunne, L. & Eales, S. A. The SCUBA Local Universe Galaxy Survey – II. 450- $\mu$ m data: evidence for cold dust in bright IRAS galaxies. *Mon. Not. R. Astron. Soc. Lett.* **327**, 697–714 (2001).
58. Chapin, E. et al. An AzTEC 1.1 mm survey of the GOODS-N field – II. Multiwavelength identifications and redshift distribution. *Mon. Not. R. Astron. Soc. Lett.* **398**, 1793–1808 (2009).
59. Magnelli, B. et al. A Herschel view of the far-infrared properties of submillimetre galaxies. *Astron. Astrophys.* **539**, 155 (2012).
60. Simpson, J. et al. The SCUBA-2 Cosmology Legacy Survey: multi-wavelength properties of ALMA-identified submillimeter galaxies in UKIDSS UDS. *Astrophys. J.* **839**, 58 (2017).
61. Da Cunha, E. et al. On the effect of the cosmic microwave background in high-redshift (sub-)millimeter observations. *Astrophys. J.* **766**, 13 (2013).
62. James, A., Dunne, L., Eales, S. & Edmunds, M. SCUBA observations of galaxies with metallicity measurements: a new method for determining the relation between submillimetre luminosity and dust mass. *Mon. Not. R. Astron. Soc. Lett.* **335**, 753–761 (2002).
63. Dunne, L., Eales, S., Ivison, R., Morgan, H. & Edmunds, M. Type II supernovae as a significant source of interstellar dust. *Nature* **424**, 285–287 (2003).
64. Da Cunha, E. et al. An ALMA survey of sub-millimeter galaxies in the Extended Chandra Deep Field South: physical properties derived from ultraviolet-to-radio modeling. *Astrophys. J.* **806**, 110 (2015).
65. Solomon, P. & Vanden Bout, P. Molecular gas at high redshift. *Ann. Rev. Astron. Astrophys.* **43**, 677–725 (2005).
66. Scoville, N. et al. ISM masses and the star formation law at  $z=1$  to 6: ALMA observations of dust continuum in 145 galaxies in the COSMOS survey field. *Astrophys. J.* **820**, 83 (2016).

67. Papadopoulos, P. P. et al. The molecular gas in luminous infrared galaxies. II. Extreme physical conditions and their effects on the Xco factor. *Astrophys. J.* **751**, 10 (2012).
68. Engel, H. et al. Most submillimeter galaxies are major mergers. *Astrophys. J.* **724**, 233–243 (2010).

### Acknowledgements

We thank I. Smail for insightful comments that improved the quality of the paper. J.A.Z. acknowledges support from a Mexican Consejo Nacional de Ciencia y Tecnología studentship. R.J.L., L.D. and I.O. acknowledge support from the European Research Council in the form of the Advanced Investigator Programme, 321302, COSMICISM. L.D. additionally acknowledges support from the European Research Council Consolidator Grant CosmicDust. H.D. acknowledges financial support from the Spanish Ministry of Economy and Competitiveness under the 2014 Ramón y Cajal programme MINECO RYC-2014-15686. M.J.M. acknowledges the support of the National Science Centre, Poland through the POLONEZ grant 2015/19/P/ST9/04010 and the European Union's Horizon 2020 research and innovation programme under the Marie Skłodowska-Curie grant agreement number 665778. This work would not have been possible without long-term financial support from the Mexican Consejo Nacional de Ciencia y Tecnología during the construction and early operational phase of the Large Millimeter Telescope Alfonso Serrano, as well as support from the United States National Science Foundation via the University Radio Observatory programme, the Instituto Nacional de Astrofísica, Óptica y Electrónica and the University of Massachusetts. The SMA is a joint project between the Smithsonian Astrophysical Observatory and the Academia Sinica Institute of Astronomy and Astrophysics, and is funded by the Smithsonian Institution and the Academia Sinica. ALMA is a partnership of the European Southern Observatory (representing its member states), National Science Foundation (USA) and National Institutes of Natural Sciences (Japan), together with the National Research

Council (Canada), Ministry of Science and Technology and Academia Sinica Institute of Astronomy and Astrophysics (Taiwan), and Korea Astronomy and Space Science Institute (Republic of Korea), in cooperation with the Republic of Chile. The Joint ALMA Observatory is operated by the European Southern Observatory, Associated Universities/National Radio Astronomy Observatory and National Astronomical Observatory of Japan.

### Author contributions

J.A.Z. led the scientific analysis and the writing of the paper, as well as the SMA follow-up proposal. R.J.L., E.V., S.E., A.C., H.D., J.S.D., L.D., M.J.M., S.S., M.W.L.S. and P.v.d.W. contributed to the original Herschel proposals and observations, by which this source was discovered and catalogued. A.M., D.H.H., E.V., I.A., V.A.-R., M.C., D.R.G., E.T. and O.V. performed the selection of the sample for the LMT observations and led the LMT proposals. M.S.Y., G.N., F.P.S., G.W.W., D.S.-A., A.V. and M.Z. carried out LMT data reduction and interpretation. D.W., M.S.Y. and A.I.G.-R. assisted with the SMA observations and data reduction. J.S., I.O. and H.N. contributed to the data analysis and fitting and modelling the results. All the authors discussed and contributed to the writing of the paper.

### Competing interests

The authors declare no competing financial interests.

### Additional information

**Reprints and permissions information** is available at [www.nature.com/reprints](http://www.nature.com/reprints).

**Correspondence and requests for materials** should be addressed to J.A.Z.

**Publisher's note:** Springer Nature remains neutral with regard to jurisdictional claims in published maps and institutional affiliations.